

Chapter 13

Coherent Light Sources in the Extreme Ultraviolet, Frequency Combs and Attosecond Pulses

Matt Zepf

Abstract Converting laser radiation into coherent extreme ultraviolet radiation via high-order harmonic processes allows the creation of extremely broadband spectra with well-behaved phase structure. Such spectra will exhibit attosecond temporal structure – either in the form of an attosecond pulse train or an isolated attosecond pulse. The basic principles of achieving such broad, phase controlled spectra and the two prevalent non-linear media (extended gaseous media and step-like plasma-vacuum interfaces) will be discussed.

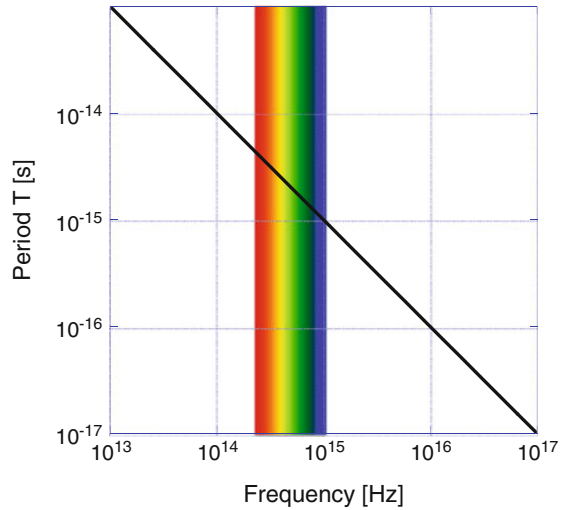
13.1 Introduction

The history of science and human discovery is also a history of describing and recording nature to develop and communicate scientific theories and concepts. The strong influence of vision on how we perceive the world around us makes images of natural processes extremely powerful in shaping our understanding of the world. Thus it comes as no surprise that using lenses as a means of enhancing our vision (as magnifying glasses) dates back to Greek and Roman times. The impact of using pairs of glass lenses to form telescopes by Galileo challenged and led to a transformation of our worldview. However, the recording of what was observed had to be performed by hand with its obvious limitations in terms of speed and accuracy. Since the development of the first photographic materials in the early part of the nineteenth century by Niépce and Daguerre, photographic recording has undergone an extremely rapid development, culminating in pixelated semi-conductor devices such as CCDs (charge-coupled devices), which allow rapid acquisition and storage of digital images. Digital images are not only a simplification of the processes

M. Zepf (✉)

School of Mathematics and Physics, Queen's University of Belfast, BT7 1NN, UK
e-mail: m.zepf@qub.ac.uk

Fig. 13.1 Single cycle limit vs. carrier frequency. Note that achieving pulse durations below 1 fs requires frequencies beyond the optical spectrum



possible until then, they are also the essential ingredient to novel forms of microscopy using high quality X-ray beams for lensless microscopy and hence the reconstruction of objects on a nm to scale [1], which can also be combined with femtosecond (10^{-15} s) temporal resolution. To achieve recording on such extreme temporal and spatial scales requires a photon source, that can provide sufficiently well controlled (coherent, short) pulses of light. Thus, extending the realm of natural phenomena that can be investigated using photons relies as much on the development of light sources as on the development of suitable detection systems. In particular recording dynamic events without motion blurring requires either a bright continuous light source combined with a detector with sufficient temporal resolution (shuttering/gating) or a slow detector with a bright sufficiently short pulse light source. Note that the two approaches differ substantially in terms of what can realistically be achieved. While mechanical shutters are ultimately limited (by inertia) to shutter speeds of around a microsecond and electrically gated shutters are limited to temporal windows of 50–100 ps by the risetime of the electrical pulses driving them, the limit for photon light sources is simply given by the Fourier-transform limit of the spectral width of the pulse. Thus the ultimate limit for a given pulse of a frequency f is a temporal duration of the associated optical cycle $T = 1/f$.¹ Figure 13.1 shows the duration of a single optical cycle vs. the centre frequency.

What is clear from Fig. 13.1 is that the shortest pulse duration that can be achieved using optical pulses is limited to just above 1 fs. While this is an extremely short pulse, it is still long compared to the dynamics of a bound electron. For

¹Note that the temporal resolution of electrically gated devices such as Pockels cells and gated MCPs is also limited by the effective bandwidth of the electrical signals and their dispersion.

example the timescale associated with the Bohr-orbit in the ground state of hydrogen is $\tau_{Bohr} = v/r_{Bohr} = 2.4 \times 10^{-17} \text{ s} = 24 \text{ as}$ (also known as the atomic unit of time). Consequently, freezing the dynamics of electrons under such conditions requires pulses in the attosecond regime and therefore light pulses in the extreme ultraviolet part of the electromagnetic spectrum and beyond [2–4].

13.1.1 Requirements for Attosecond Pulses

The challenge is therefore to generate and control light under such conditions. To understand the requirements that we need to meet, it is useful to first recap how ultrafast pulses close to the single cycle limit are generated using optical lasers. The first condition that needs to be met by any light source that aims to be shorter than a given pulse duration is that the bandwidth must be sufficiently large to support the pulse duration. The Fourier transform limit of a given spectrum is given by $\Delta\nu\Delta t = \beta$, whereby β is constant of the order of unity that depends on the exact spectral shape. For example, for a Gaussian spectral shape $\beta = 0.441$, while a sech^2 has $\beta = 0.315$.

While large spectral bandwidth is a necessary requirement, it is clearly not sufficient (think of a light-bulb!). The key parameter that distinguishes a light-bulb from a femtosecond optical pulse is the spectral phase. The Fourier-transform limited pulse duration is only achieved if the phase of all spectral components is identical. Hence, one needs to find a means of producing a broad spectrum with identical spectral phase. In the optical regime, the characteristics of our light pulse are controlled by designing the optical cavity to ensure that only those photons that match our requirements are allowed to propagate in the oscillator, while the unwanted photons have a net-loss in each round-trip and thus die away exponentially.

Remember that oscillator cavities only support discrete frequencies (oscillator modes) separated by a frequency $\Delta\nu_{comb} = c/2L$ (i.e. the cavity round-trip length $2L$ is a multiple of the wavelength λ). Hence an oscillator produces a comb of equally spaced spectral peaks. In time, such a frequency comb with constant spectral phase corresponds not to a single short pulse but a *pulse train* (Fig. 13.2) [5, 6]. That this should be the case is also easily understood from the basic layout of an oscillator which contains a pulse that is short compared to the cavity length (Fig. 13.3). Every time the pulse reflects from the partial reflector, part of the pulse is also transmitted and the separation between each of the transmitted pulses must just be the cavity round-trip time of the oscillator. The task of achieving a transform limited pulse is therefore equivalent to achieving a fixed relative phase between the individual modes of the oscillator – a mode-locked frequency comb. For a reflective cavity with no dispersive elements this will be fulfilled to very good approximation. However a laser cavity must include a gain medium, which contributes dispersion (i.e. frequency dependent phase) to the cavity and thus results in the phase between two modes varying from one round-trip to the next. To regain the fixed relative phase

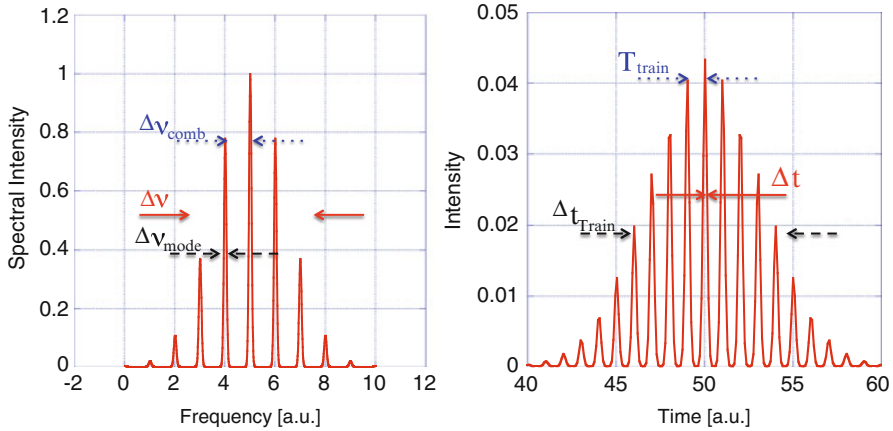


Fig. 13.2 Fourier-transform of a frequency comb under the assumption of ideal (constant) spectral phase. Note the correspondence between spectrum and time of the various structures, with corresponding features in frequency and time highlighted by corresponding colour and lines. The temporal duration of each attosecond spike $\Delta t \Delta v$ is set by the total spectral width Δv (solid line), the separation of each peak in the frequency comb Δv_{comb} (i.e. mode-separation or harmonic separation) determines the period of pulse-train T_{train} (dots) while the width of each individual (harmonic or mode) peak Δv_{mode} determines the temporal width of the train as a whole Δt_{train} (dashed line)

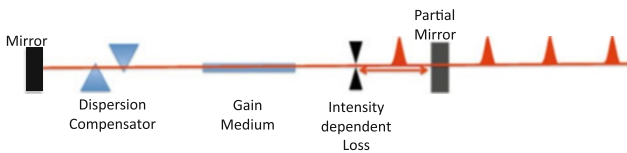


Fig. 13.3 Schematic of a mode-locked oscillator showing the key components required for operation. The dispersion compensator (shown here as a prism pair) ensures that the relative spectral phase of each mode stays constant from one round-trip to the next. The intensity dependent loss mechanism (shown here as an aperture placed at the focus of a Kerr-lens) ensures that only intense pulses can propagate through the cavity with a net gain. The separation of the peaks in the pulse-train transmitted through the partial mirror corresponds to one oscillator round-trip in reality

between these modes (i.e. mode-locked operation), a short pulse cavity must include additional dispersive elements that compensate the dispersion in the gain medium. Common approaches to achieving this goal are a prism-pair or dispersive (‘chirped’) mirrors (Fig. 13.3). Compensating the dispersion allows the relative spectral phase of the modes to remain fixed. It does not, however, result in the selection of modes with identical spectral phase. Since the shortest pulse for a given average power in the oscillator cavity corresponds to the highest peak intensity, the selection of a short pulse is achieved by introducing an intensity dependent loss mechanism (such as a Kerr-lens with an aperture at its focus or a saturable absorber).

It is easy to see that such an optical layout will produce a pulse-train of ultra-short pulses with a repetition rate corresponding to the cavity round-trip time $T_{train} = 1/\Delta\nu_{comb} = 2L/c$. For time resolved applications using an isolated pulse is of course highly desirable. In the optical regime selecting a single pulse from such an oscillator can be straightforwardly achieved by electro-optical switching using a Pockels-cell, since typical cavity round-trip times (and therefore interpulse spacings) are ~ 10 ns. The changed temporal structure (by selecting a single pulse) must result in a change of the spectral structure. Selecting a single pulse corresponds to a pulse-train with infinite spacing. Since the separation of the pulses in time is inversely proportional to the comb-spacing in frequency, we obtain $\Delta\nu_{comb} = 0$ and hence a continuous spectrum.

At this point it is worth emphasising some basic corollaries from our discussion (Fig. 13.2).

1. Although the lasing medium produces, and can amplify, emission from a continuous range of frequencies the temporal interference in a cavity results in a spectral structure commonly referred to as a frequency comb.
2. Achieving constant spectral phase across the frequency comb results in the individual pulses having a duration corresponding to the Fourier Transform Limit.
3. Isolating a single pulse from the train changes the spectrum from a frequency comb to a continuous spectrum while retaining the same shape of the envelope.
4. The temporal separation of the pulses is connected to the frequency separation of the individual modes as $T_{train} = 1/\Delta\nu_{comb}$
5. The temporal duration of each pulse in the train is determined by the width of the spectral envelope $\Delta t = \beta/\Delta\nu$
6. The width of the temporal envelope in the pulse-train Δt_{train} is determined by the spectral width $\Delta\nu_{mode}$ of the individual frequency comb spikes

13.2 Producing an Attosecond Pulse – Harmonic Generation

From the previous discussion it is clear that scaling the principle of a femtosecond oscillator to an attosecond pulse(-train) requires the production of a phase-locked frequency distribution (-comb) with an overall spectral width $\Delta\nu$ sufficient to support the desired pulse-duration. Once this has been achieved the remaining challenge is to isolate an individual pulse from the train (or to ensure only one is produced in the first instance). As can be seen from Fig. 13.1 achieving a pulse duration below 100 as requires a central frequency of $> 10^{16}$ Hz or expressed in terms of wavelength of < 30 nm. The lack of optical components with similar quality to those found in visible/infra-red lasers in terms of reflectivity and transparency and the lack of easily pumped gain media result in the oscillator approach developed at optical wavelengths no longer being directly applicable.

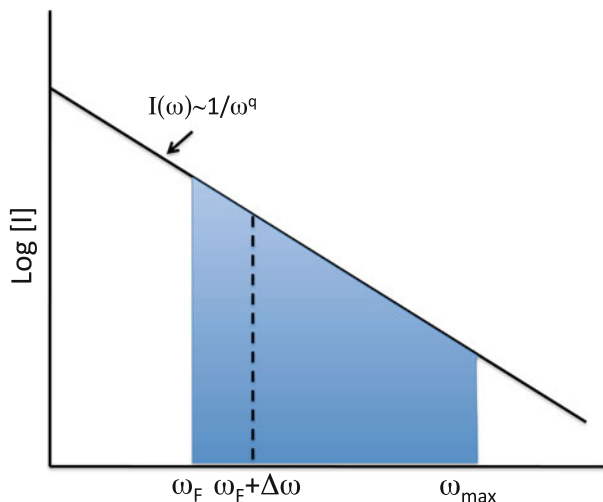
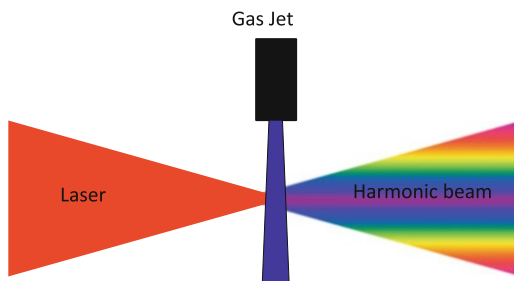


Fig. 13.4 Schematic of a harmonic spectrum with power-law decay ω^{-q} (plotted with both axes logarithmic). The spectral width and hence the Fourier-transform limited pulse duration is determined only by the low-frequency cut-off of the filter ω_F and the parameter q

However the principles derived from mode-locked oscillators still apply. The frequency comb technique is extended to short wavelength by generating harmonics (integer multiples) of the laser frequency at frequencies $\omega_m = m\omega_{Laser}$. Harmonics can be generated in any medium that displays a strong non-linear response to the incident laser light. Consider an electron bound in an atomic potential: as long as the potential shape is parabolic to good approximation, the electron will respond as a simple harmonic oscillator, which oscillates and emits light only at the frequency of the incident light wave. Since all atomic potential wells are parabolic to good approximation for sufficiently small amplitudes (cf. Taylor expansion), the polarisation at low intensities is simply linear with the applied electric field $\mathbf{P}^{(1)} = \epsilon_0 \chi^{(1)} \mathbf{E}$ and the superposition of the external and re-emitted field results in the well-known linear refractive index n . At higher intensities the potential shape generally deviates from an ideal parabola and the polarisation of the medium contains higher order terms $|P^{(n)}| \sim \chi^{(n)} E^n$. In terms of the electron's motion this simply implies that the electron's displacement x must be described as a series that requires higher frequencies $2\omega, 3\omega, \dots, n\omega$ to describe the motion and the emitted field accurately, and thus the emission of higher integer multiples of the laser frequency (harmonics). However, the production of harmonics on its own is not sufficient to achieve as substantial reduction of the pulse duration. To lead to a substantial increase in the effective bandwidth harmonic spectrum must decay sufficiently slowly. Assuming a simple power law decay of a given spectrum [7], such that $I(\omega) \sim 1/\omega^q$ and a simple step filter that transmits above some critical frequency ω_F one obtains an effective bandwidth of the spectrum collected by the filter of $\Delta\omega = (2^{1/q} - 1)\omega_F$ (Fig. 13.4). Note that the transform limited pulse duration is purely determined by

Fig. 13.5 Schematic of a simple HHG experiment with a gaseous non-linear medium. Typical parameters would be lasers with few to 10's of optical cycles with intensities close to the saturation intensity for tunnel-ionisation for the medium of interest (typically 10^{14} – 10^{15} W cm $^{-2}$)



the decay of the spectrum and the lowest transmitted frequency ω_F . Any constraint on the maximum frequency ω_{max} in the transmitted spectrum has no bearing on the pulse duration, so long as $\omega_{max} > \omega_F + \Delta\omega$.

While harmonics generated from bound electrons via the perturbative process described above find widespread use in the frequency doubling of lasers in crystals and even some higher order direct processes in gases such as 3rd harmonic generation, their intensity generally decays too rapidly to higher orders to be a source of a broad harmonic frequency comb suitable for producing a higher central frequency with increased spectral bandwidth. Note that bulk solid media can be ruled out as a suitable non-linear medium for attosecond pulse generation, because they strongly absorb the high frequencies required for attosecond pulse production. Therefore we will need to look beyond the perturbative harmonic generation from bound electrons i.e. consider laser fields comparable or large with respect to the binding field strength and consider only gaseous media or surfaces.

13.2.1 *Non-Linear Medium 1: Harmonic Generation from Gaseous Targets (HHG)*

As the intensity is increased further – e.g. by placing a jet of atoms into the focus of a femtosecond laser (Fig. 13.5) – to an appreciable percentage of the Coulomb field of the atom, the perturbative approximation breaks down, because the electron is no longer trapped in the potential well of the atom, but can instead tunnel ionise. Once ionised the electrons motion can be described to good approximation by the motion of a free electron in the laser field [8]. For linear polarisation there is a high probability that the electron will recollide with the atom and emit a photon with an energy of $h\nu = I_p + W_{kin}$ (where I_p is the ionisation potential, W_{kin} the kinetic energy of the returning electron). By solving the equation of motion for an electron that tunnel ionises at a time t_0 in a field given by $E(t) = E_0 \cos(\omega t)$ one finds that the electrons velocity at a given point in time depends on t_0 as

$$v(t, t_0) = -\frac{eE_0}{m\omega} [\sin(\omega t) - \sin(\omega t_0)] \quad (13.1)$$

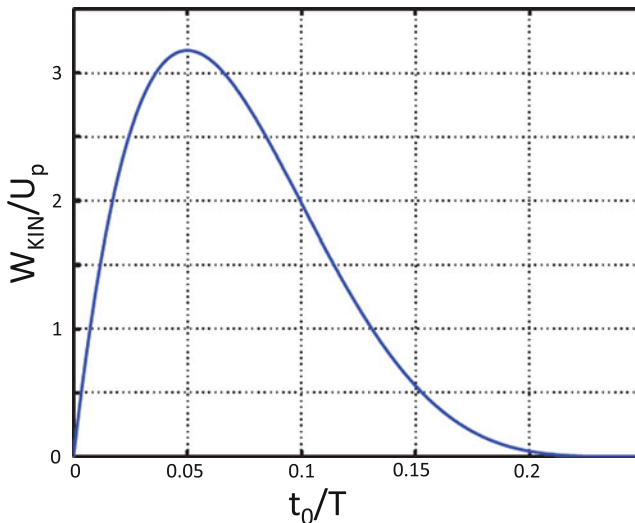


Fig. 13.6 Kinetic energy upon first return versus tunnelling time in units of the laser period T . The maximum possible return energy is $3.17 \times$ the ponderomotive energy U_p . Note that for all return energies apart from $3.17U_p$ two distinct tunnelling times exist that lead to the same return energy, corresponding to the long and short trajectories respectively. The pattern repeats in the second half-cycle $t_0/T > 0.5$. Note that not all tunnelling times t_0 lead to solutions that return to the parent ion within the first optical cycle

The return energy therefore also depends on t_0 and reaches a maximum value of $W_{kin} = 3.17U_p$ for electrons which ionise 17° after the peak of the electric field of the laser (Fig. 13.6, where the ponderomotive energy $U_p = e^2E^2/m\omega^2 = 9.33 \times 10^{-14}I[\text{Wcm}^{-2}]\lambda^2[\mu\text{m}^2]$ is the kinetic energy of a free electron oscillating in the laser field). Therefore the highest possible photon energy is given by the sum of the kinetic energy and the ionisation potential.

$$h\nu_{max} = I_p + 3.17U_p \quad (13.2)$$

Thus, harmonic generation in the tunnel-ionising regime is generally thought of as a three-step process [8]:

1. Electron tunnel ionises
2. Electron gains energy in the laser field
3. Harmonic photons are emitted upon recombination with the atom

Unlike perturbative harmonic generation discussed earlier, the probability of generating a photon at a given harmonic order m , is only weakly dependent on the harmonic order. We might expect photon energies that correspond to electrons ‘born’ at the peak of the field, where the ionisation rate is highest (Fig. 13.7), to be somewhat stronger and thus favouring higher harmonic orders. However this effect is off-set by the fact that the recombination probability is higher for electrons with

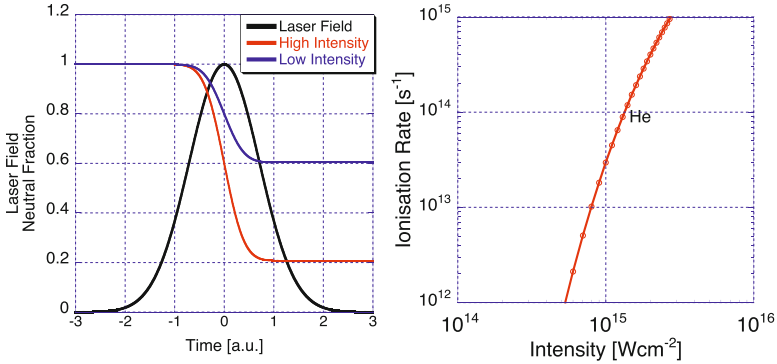


Fig. 13.7 Temporal dependence of ionisation fraction (*left*) and intensity dependence of ionisation rate (*right*). The remaining neutral fraction at the peak of the pulse strongly depends on the pulse intensity

lower return energy, resulting a slow decay of the harmonic spectrum (Fig. 13.9). As discussed earlier, the effective bandwidth of a slowly decaying frequency comb can be very large and would be sufficient for transform limited pulses of 10's of attoseconds. Note that harmonics are generated twice per optical cycle with a separation of $T/2$, since the ionisation dynamics are symmetrical with respect to the sign of the electric field. From our previous discussion on laser cavities we see that harmonics must therefore be separated by $\Delta\nu = 2/T = 2\nu_{\text{Laser}}$ and therefore only odd harmonic orders $n = 1, 3, 5$, are generated. From the physical picture of the dynamics on a single atom level described above, it may seem surprising that one observes emission of well defined harmonics at all. Since electrons can return with a continuum of energies $W_{\text{kin}}(t_0) = 0 \dots 3.17U_p$ one might expect to observe the emission of a continuous photon energy spectrum instead of a discrete frequency comb. However we can easily see that even harmonic orders generated in one half-cycle are simply cancelled by destructive interference with the even harmonics generated in the following half-cycle. The interference between waves generated in each half cycle also explains the observation of well-defined harmonics per se. Similar to a Fabry-Perot etalon, the sharpness of a peak increases with increasing number of interfering beams or, in our case, an increasing number of attosecond pulses. Therefore the appearance of odd harmonics can be understood as interference between the individual attosecond pulses in the pulse train. Isolating a single attosecond pulse from this train must therefore result in a continuous spectrum being observed as is indeed the case.

13.2.1.1 Short Wavelength Limit of HHG

From Eq. 13.2 it is clear that to produce harmonics with the shortest wavelength requires the highest possible value of both U_p (and therefore $I\lambda^2$) and I_p . However,

these two parameters are not independent of each other, and the maximum possible value of U_p depends on I_p and the pulse duration. Since ionisation is an intrinsic part of the HHG process, the medium (typically a neutral noble gas or noble gas ion) will become depleted during the laser pulse (Fig. 13.7). The maximum intensity I_{SAT} for a given species is given by the point where the remaining amount $N(I)$ of the generating species at the peak of the pulse falls below a given threshold (e.g. $N(I_{SAT})/N_0 < 1/e$). The dominant ionisation mechanism for HHG experiments typically tunnel ionisation, which is well approximated by the ADK formula (Ammosov, Delone, Krainov [9]). Figure 13.7 shows the tunnel ionisation rate as a function of intensity. It is clear that even for very short pulses the ionisation probability will rapidly approach unity during the laser pulse even for moderate intensities.

$$W = \int R(t)dt \sim \frac{R_{I_{max}}\tau}{2} \quad (13.3)$$

Figure 13.7 shows the temporal dependence of ionisation during a laser pulse. For the higher intensity pulse the cumulative ionisation during the pulse has significantly depleted the neutral species before the peak of the pulse, while for the lower intensity pulse most atoms remain neutral. While HHG from ions [10] is possible, it is much harder to achieve a strong response from the entire medium due to macroscopic phase-matching considerations discussed below. The strong preference for neutral media arising from this makes the neutral atoms with the highest ionisation potentials the preferred choice as HHG medium (He 25.4 eV, Ne 21.6 eV, Ar 15.8, Kr 14 eV, Xe 11 eV). Equation 13.2 suggests that the use of long wavelengths can be used to extend the cut-off for neutral media by using very long laser wavelengths. While this is indeed true and photon energies exceeding 1 keV have been produced with long wavelength lasers, the benefit of this approach is offset to a certain degree by the strong wavelength scaling of harmonic emission probability $P \propto \lambda^{-6}$ [11]. This scaling can be understood in qualitative terms to be due to wave packet spreading after ionisation reducing the amplitude of the electron wave function at the point of recollision and thus substantially reducing the recollision probability. This dependence on the wave packet evolution between ionisation and recollision points to the importance of the 2nd phase of the 3-step process in understanding the behaviour of HHG.

13.2.1.2 HHG Phase

Thus HHG from gaseous targets appears to be a promising route to generating attosecond pulses. However, before we consider our quest for an attosecond pulse complete we must first consider the phase structure of the harmonics, the route to achieving appreciable conversion efficiencies and selection of a single attosecond pulse. For perturbative harmonics generated from bound electrons, the phase of the harmonic is essentially dictated by that of the driving laser. In this case we can view the harmonic generation process as a strongly driven oscillator, where the relative

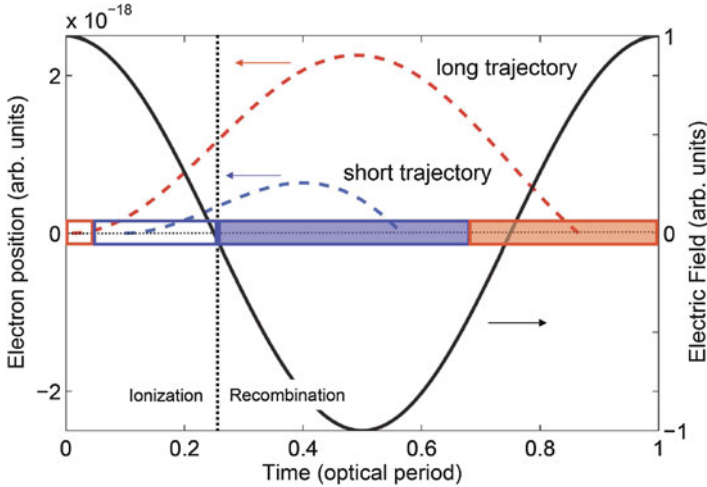


Fig. 13.8 Illustration of the two distinct electron trajectories in HHG. Times of ionisation and recombination for the long (larger area) and short (smaller area) trajectory in a laser field (solid curve). Two example trajectories are highlighted for a short trajectory ionised at $t_0 = 0.1$ and long trajectory ionised at $t_0 = 0.01$ (dashed curves). They are plotted as electron position with respect to the parent ion vs. time

phase between the driving force and the electron oscillation depends only on the ratio of the laser frequency to the resonance frequency of the oscillator. For HHG generated via the 3-step process described above, the situation is significantly more complex. From a purely classical view of the electron trajectory after ionisation, it is clear that the time of recombination depends on the laser phase at the point of ionisation and hence the time elapsed between ionisation and recombination is a function of the emitted photon energy, implying that we would expect a chirp in the spectrum of each individual attosecond burst. Close inspection of the equations of motion shows that during an optical half-cycle all return energies can occur for 2 distinct values of ionisation phase, with the exception of the cut-off energy, which only occurs for a single well defined value of t_0 (Fig. 13.6). These distinct quantum paths are referred to as the long and short trajectory respectively (Fig. 13.8) and for each trajectory the relative phase between the harmonic and the laser must be different since they relative phase clearly depends on the time of return t_R . The full quantum mechanical picture must take into account the phase of the electron wavepacket, which is proportional to the quasi-classical action integral along the path of the free electron $S(t_0, t_R)$ [12].² The accumulated phase of the electron is

$$\phi(m) = m\omega t_R - \frac{1}{\hbar}S(t_0, t_R) \quad (13.4)$$

²The action is the product of electron energy and time.

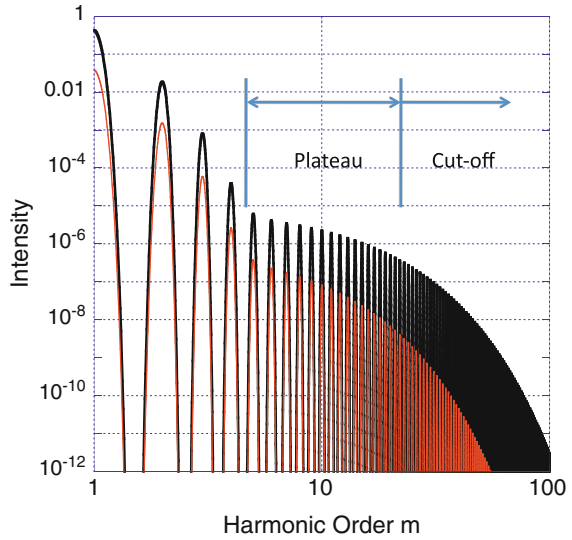
This distinct emission phase for short and the long path results in interference between the two quantum paths. In practise, optimising the conversion efficiency and selecting an isolated attosecond pulse requires phase matching (discussed below), which automatically results in the selection of one quantum path over the other. For the further discussion it is always assumed that one quantum path is being selected via phase matching. However, the fact that relative phase between the harmonic and the laser depends on the time and mean energy between ionisation and recollision, implies a different phase for each harmonic order. Therefore the HHG spectrum is intrinsically chirped and thus the attosecond pulses in the train are longer than the FTL. Controlling this chirp requires the use of suitably dispersive filters or chirped (dispersive) XUV multi-layer mirrors.

13.2.1.3 Isolating a Single Attosecond Pulse

For time-resolved experiments having only one pulse greatly simplifies the measurement and hence one would like to find a way to isolate a single attosecond pulse. Applying an optical switch as in the case of a mode-locked oscillator separately from the production of the pulse-train appears impractical because the temporal separation of the individual pulses is extremely short. In practise therefore the selection of an individual attosecond pulse is performed by controlling the properties of the laser generating the harmonics. There are two main approaches to isolating an individual attosecond pulse:

- (i) Intensity gating: For very short pulses (~ 5 fs) the neighbouring optical half-cycles relative to the peak cycle already have an appreciable lower intensity. The intensity dependence of the HHG process is mainly determined by the tunnel ionisation rate $R(I)$, which can be approximated as $R \propto I^5 \dots I^7$ in the regime of interest. This implies a strong suppression of the neighbouring half cycle in terms of conversion efficiency. Secondly, the cut-off harmonic scales linearly with I , implying that there is a spectral region which is only produced by the strongest half-cycle (Fig. 13.9). In this spectral region only a single burst of XUV radiation is produced during each pulse and thus an appropriate filter or multi-layer mirror can be used to select the desired spectral range [13].
- (ii) Polarisation gating: For longer pulses, the efficiency from one cycle to the next can be controlled by exploiting the polarisation dependence of the HHG process [14, 15]. The strong reduction in efficiency with ellipticity of the laser light can be understood in terms of the trajectory of the free electron in the laser field. In the case of circular polarisation the electrons will not generally return to the parent ion and hence no XUV photons are emitted. If a laser pulse with time varying ellipticity $\varepsilon(t)$ can be produced it will only produce harmonics efficiently for those cycle which are close to linearly polarised, i.e. $\varepsilon(t) \sim 0$. Such a polarisation state can be produced by superimposing two delayed pulses with left- and right-circular polarisation respectively. For sufficiently short pulses the laser will only be linearly polarised for one half-cycle, resulting in the emission of an isolated attosecond pulse.

Fig. 13.9 Typical harmonic spectrum exhibiting rapid decay to a plateau region and exponential cut-off. The two spectra are similar except for the strength and position of the cut-off corresponding to a spectrum generated with lower intensity (red) and higher intensity (black) for a few cycle laser. If the cut-off region of the black spectrum is uniquely produced by one cycle it becomes spectrally continuous and with suitable filtering will result in an isolated attosecond pulse (Color figure online)



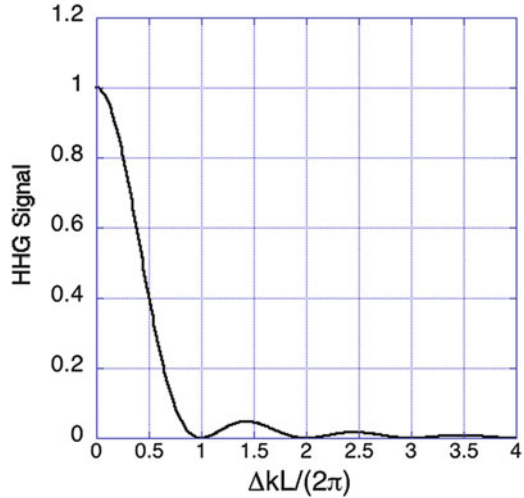
13.2.1.4 The Role of Phase Matching

The macroscopic response of the medium must depend on the coherent sum of all emitters at the point of the observer [16]. Clearly achieving the maximum harmonic signal therefore requires that all emitters add in phase, or at the very least, not destructively i.e. with a phase difference of $< \pi$. For perfect coherent overlap of the fields emitted from N individual atoms, the electric field will simply be $E = NE_{atom}$ and the measured intensity $I \propto N^2$. The total number of atoms contributing to the harmonic signal is simply $N = n_a LA$, where n_a is the atomic density, L the length and A the effective area of the focal spot. Including the probability of a harmonic photon being emitted for a given atom P_m , the maximum achievable intensity is therefore $I(m) \propto (n_a LAP_m)^2$. For otherwise fixed parameters, the effective length L_{eff} is limited to either

- the maximum length L_I over which a sufficiently high intensity can be maintained (usually due to defocusing or absorption of the laser radiation)
- the absorption length $L_{abs} = (n_a * \sigma)^{-1}$ of the harmonic radiation [16], where σ is the absorption cross-section.
- the coherence length L_c by dispersion between the harmonic and the laser field.

The coherence length $L_c = \pi/\Delta k$ is the length over which a signal can grow without destructive interference in extended non-linear medium, where $\Delta k = k_m - mk_{Laser}$. Here m is the harmonic order k_i is the wave vector of the harmonic or laser respectively. Clearly in vacuum $k_m = mk_{Laser}$ and one has perfect phase matching $\Delta k = 0$. In the presence of a medium the phase matching corresponds to the harmonic and the laser driving the interaction having identical phase velocities and therefore an identical refractive index n . The effect of any mismatch $\Delta k > \pi$ is very substantial and the phase matching form-factor $F(\Delta k)$ is shown in Fig. 13.10.

Fig. 13.10 Phase matching factor $F(\Delta k)$ as a function of phase mismatch ΔkL . Note the rapid decay beyond a total mismatch of π radians



Phase matching can only be achieved over a narrow time window, since the continuous ionisation of the medium leads to time varying contributions to the dispersion (Figure 13.7). Optimised harmonic generation can thus be summarised by achieving phase matching over the maximum possible length allowed by absorption L_{abs} at the peak of the laser pulse. The ideal choice of medium (in the presence of phase-matching) is therefore determined by optimising the ratio P/σ .

In practice, all dispersive terms are wavelength dependent and thus phase matching can in principle only be achieved by balancing the different contributions to the dispersion. The wavelength dependence of the dispersive terms implies that one would expect this to be exactly possible for only one wavelength, though achieving $L_c > L_{abs}$ may be possible over a fairly wide range of wavelengths. In practice, the refractive index for the high order harmonic can be assumed to be $n_m = 1$. In the case of phase matching in a capillary waveguide phase matching is dominated by laser propagation effects [17]

$$k_{Laser} \approx \frac{2\pi}{\lambda} + \frac{2\pi p(1-\eta)\delta(\lambda)}{\lambda} - p\eta N_{atm} r_e \lambda - \frac{u_{11}^2 \lambda}{4\pi a^2} \quad (13.5)$$

where the terms are the vacuum k-vector, the neutral atom dispersion, the plasma dispersion and the waveguide dispersion (with p : pressure in *atm* η : ionisation fraction, N_{atm} : number density at 1 atmosphere, r_e : classical electron radius, δ : neutral gas dispersion).

In free propagating geometries the waveguide dispersion term would be replaced by the Guoy shift [18] which has the useful property of changing sign in the focus. For all practically relevant circumstances, the dominant term with $(n-1) < 0$ is the refractive index due to free electrons while the leading term with $(n-1) > 0$ is refractive index of the neutral atoms. As a rule of thumb, the free electron dispersion is around 20–50 \times greater than that neutral dispersion of the gas thus implying

that phase matching should be achieved at ionisation levels of a few % [17]. This constrains the highest harmonic that can be achieved due to Eq. 13.2 and thus is applicable only to harmonic orders up to 30 using a Ti:Sapphire laser at 800 nm and that phase matching ions with a charge state $Z > 1$ is impossible since no neutral atoms are available to balance the dispersion of the free electrons. The λ^2 scaling of the cut-off allows phase matching using this approach to be extended to shorter wavelengths, but at the cost of a much weaker ($P \sim \lambda^{-6}$) single atom response and thus limited overall response [19].

13.2.1.5 Quasi-Phase Matching (QPM)

Thus, while true phase matching ($\Delta k = 0$) is desirable, it is only achievable in a narrow parameter space. Therefore optimisation of other parameters such as the laser intensity, ionisation potential and P/σ is significantly constrained by the need to maintain phase matching. So called quasi-phase matching provides an alternative to ensure rapid signal growth of harmonic radiation. The principle of quasi-phase matching is illustrated in Fig. 13.11 [20], and simply relies on suppressing the out-of-phase contributions along the propagation path. This can be done by any means, which varies the harmonic generation efficiency (intensity, medium etc.). Figure 13.11 illustrates the effect different QPM scenarios and compares these with a situation where $\Delta k \neq 0$. In the mismatched case, the signal grows for one coherence length L_c and oscillates between 0 and the maximum value achieved after one coherence length thereafter i.e. there is no advantage to using a medium longer than L_c in this case. The operating principle of QPM can be seen clearly in the ideal QPM case: The harmonic intensity initially increases for a length of L_c , for the subsequent coherence length the phase between the drive laser and harmonic field continues to slip but the overall signal level remains constant since HHG is suppressed. This process continues periodically leading to rapid signal growth. The signal will then grow quadratically with the number of QPM periods N_{QPM} (consisting of a HHG or ON zone and an suppressed or OFF zone). Recent advances have shown that interchanging noble gas with hydrogen jets allows the HHG signal to grow at the theoretical rate of N_{QPM}^2 [21] thus decoupling the challenge of phase matching from other relevant parameters.

13.2.2 Non-Linear Medium 2: Harmonic Generation from Plasma Vacuum Interfaces (SHHG)

From our initial considerations it has become clear that attosecond pulse production requires a medium with a strong non-linear response that is capable of providing a harmonic frequency comb with a well-defined phase behaviour. There are two main areas in which one would like to go beyond the performance currently available with HHG. Firstly, higher pulse energy would be highly desirable for a number of

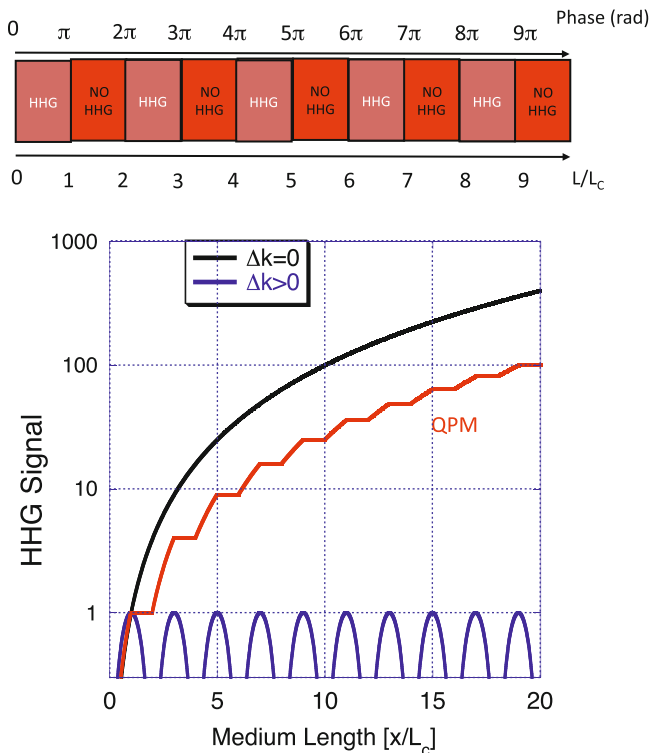


Fig. 13.11 Quasi-phase matching (QPM) allows coherent build-up of signal in the presence of wave vector mismatch ($\Delta k \neq 0$). The harmonic source term must be modulated to suppress the harmonic production over each alternate coherence length L_c (marked ‘NO HHG’) resulting in constructive interference between the HHG zones marked ‘HHG’. The signal growth for a medium with ideal QPM is compared to perfect phase matching and mismatch in the absence of QPM in the lower graph

possible applications. Secondly, the highest harmonic order that can be produced with reasonable efficiency is constrained to below a few hundred eV photon energy. The energy in a given attosecond pulse is determined by the energy of the drive laser pulse and the conversion efficiency. The conversion efficiency is quite low, owing in part to the difficulty of phase matching at shorter wavelengths and limitations on the effective density length product due to absorption and defocusing, while the low intensity required for optimal HHG of $< 10^{15} \text{ W cm}^{-2}$ makes it hard to exploit high peak powers and pulse energy available with current ultra-fast lasers. For example a 20 cm diameter petawatt power laser would require a focal length of 2 km!³ Plasma surfaces driven at relativistic intensities (SHHG) provide an attractive alternative to

³This calculation assumes a diffraction limited spot of 1 cm size and therefore a ratio of focal length to beam diameter of $f/D \sim 10^4$. While one could consider going out of focus, this is undesirable

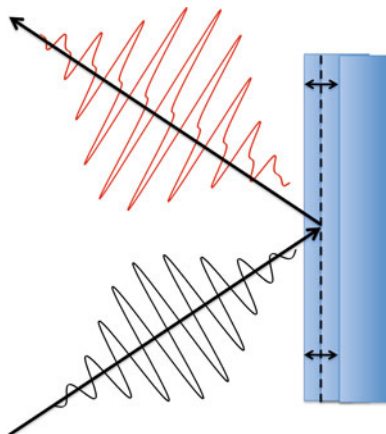


Fig. 13.12 Schematic of the Relativistically Oscillating Mirror (ROM) harmonic generation process. The force of the electric field on the plasma surface at the plasma vacuum interface leads to a periodic oscillation of the point at which the incoming laser is reflected by the plasma. This oscillation of the reflection point (indicated as a dashed line) leads to strong modification of the reflected waveform and the emission of harmonics of the laser frequency (for a multi-cycle pulse)

HHG in gaseous media and in particular a route to intense attosecond pulses. The primary mechanism of interest is the so-called Relativistically Oscillating Mirror (ROM) process, although there are other processes which can convert the optical laser light into higher orders (see [22, 23] for an in-depth reviews of SHHG).

13.2.2.1 The ROM Mechanism

Figure 13.12 shows the basic concept of up shifting via the ROM process. An initially solid target is illuminated by an intense laser with sufficiently high contrast to result in a step-like plasma vacuum interface. The plasma surface experiences the force of the laser and oscillates around its rest position with a mean kinetic energy of the order of the ponderomotive energy U_p . At high intensities, the ponderomotive potential U_p exceeds the rest-mass energy of the electron (511 keV) and the motion of the surface becomes relativistic – i.e. the surface oscillates by an appreciable fraction of a laser wavelength during each optical cycle resulting in a periodic distortion of the reflected waveform and hence harmonic generation. This occurs at $I\lambda^2 = 1.3 \times 10^{18} \text{ W cm}^{-2} \mu\text{m}^2$ and for relativistic interactions the laser strength is typically referred to by the normalised vector potential $a_0 = (I\lambda^2/1.3 \times 10^{18} \text{ W cm}^{-2} \mu\text{m}^2)^{1/2}$. Unlike the case of HHG in gaseous targets, where the electron

from the point of view of the spatial phase which tends to be excellent only in focus due to the inherent spatial filtering of the laser beam in focus.

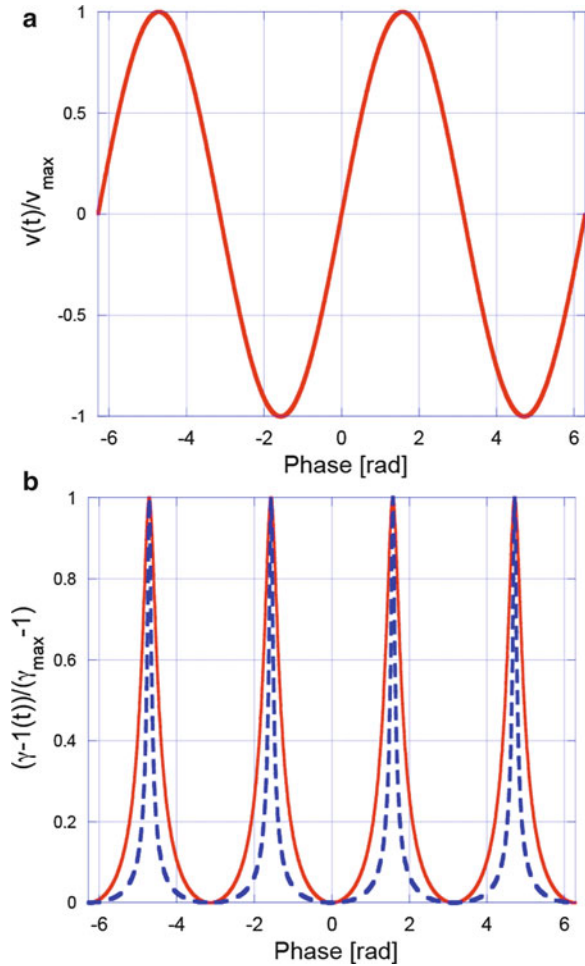
density is much less than the critical density n_c , solid targets are have $n_e/n_c \gg 1$ and hence reflect the incident laser radiation. The surface oscillations imply an oscillation of the apparent reflection point (ARP) at which the incident laser light is reflected [24, 25]. Note that even for low intensities, where the oscillation of the ARP is sinusoidal the resulting modulation and associated distortion of the phase of the reflected waveform will already give rise to harmonics. For higher intensities, the oscillation of the surface becomes increasingly non-sinusoidal giving rise to stronger harmonics. The underlying process in the case of a relativistically oscillating mirror is in many ways similar to the process of the relativistic Doppler up shift described by Einstein [26]. For a mirror moving with a constant velocity v close to the speed of light c an observer would detect reflected radiation at a frequency of $\omega_r = \omega_0(1+v/c)/(1-v/c) \approx 4\gamma^2$ (where ω_0 is the laser frequency). In the case of ROM instead of a constant value of γ describing the motion of the mirror surface, one now has Lorentz-factor that is a function of time $\gamma(t)$. The initial theoretical approach – a physical picture first proposed by Bulanov et al. [27] – was therefore to describe the harmonics observed in PIC simulations in terms of the reflection of the incident laser off a moving mirror oscillating at the laser frequency ω_0 . A detailed semi-analytical moving mirror model was developed by Lichters et al. and was found to be in good agreement with PIC simulations [24]. This demonstrated that the picture of the moving mirror captures the essence of the harmonic generation process. Experiments performed in the mid 1990s observed harmonic spectra [28,29], where the conversion efficiency $\eta(m)$ of a given harmonic order m followed a power-law scaling $\eta(n) \sim m^{-q}$, where q is an intensity dependent exponent that increased from $q = 5.5$ to $q = 3.3$ when the intensity was varied from 5×10^{17} to $10^{19} \text{ W cm}^{-2}$ [29]. A quantitative understanding of ROM spectra was first given by Gordienko et al. and Baeva et al. [25, 30], based on the dynamics of the ARP. By assuming a boundary condition for the incident and reflected electric field at the ARP $E_r + E_i = 0^4$ it was found that the harmonic spectrum assumes an asymptotic spectral shape in the so-called relativistic limit (where $\gamma_{max} \gg 1$). The spectrum retains a power law scaling for the conversion efficiency in the relativistic limit with the efficiency of the m -th harmonic reaching $\eta(m) m^{-q_{REL}}$, with $q_{REL} = 8/3$ [25]. This slow decay has been identified as being sufficient to support pulse duration in the zeptosecond regime [30] and extremely high intensity X-ray radiation [31].

13.2.2.2 Short Wavelength Limit of ROM

Naively, one would expect the short wavelength limit of ROM harmonics to be determined by the peak γ of the surface to $\omega_{max} \sim 4\gamma^2$ as predicted by the Doppler-upshift from a mirror moving at constant velocity. However the spectra,

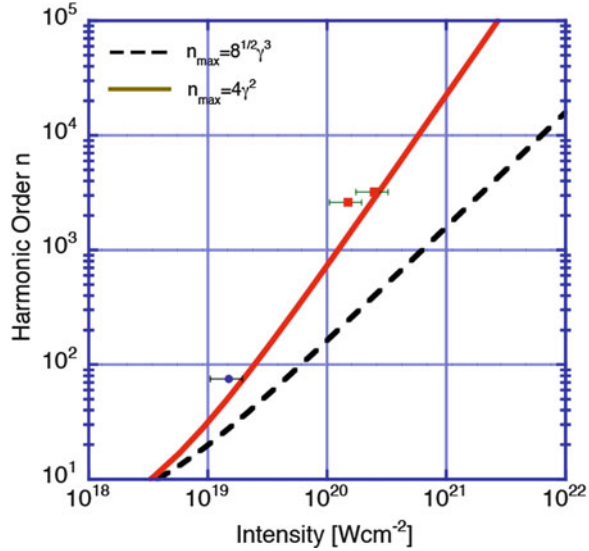
⁴This boundary condition is not always met but provides a useful guide to the typical scaling of ROM spectra [22].

Fig. 13.13 The Lorentz factor γ is sharply spiked even for a very smooth dependence of velocity with time. Here a simple sinusoidal velocity dependence ($v(\phi) = v_{max}\sin(\phi)$) is chosen to illustrate the dependence of $v(t)$ on $\gamma(t)$. The variation of the Lorentz factor for two different peak velocities $v_{max} = 0.995c$ ($\gamma_{max} \sim 6$, solid line) and $v_{max} = 0.985c$ ($\gamma_{max} \sim 22$, dashed line) is shown in the lower plot. The width of the individual γ -spikes is much less than the oscillation period and reduces linearly with increasing γ_{max}



both experimentally [32] and in simulations [25], extend far beyond this limit. The theoretical prediction is that the $q = 8/3$ scaling still applies up to an order $n_{RO} \sim 8^{1/2}\gamma_{max}^3$, beyond which the conversion efficiency decreases exponentially or rolls over. The temporal dynamics of $\gamma(t)$ are essential to understanding the substantially larger frequency up shift and hence the short wavelength limit of ROM [25, 30]. Even assuming a very smooth variation of the actual surface velocity with time (e.g. $v(t) \sim \sin(\omega t)$) as in Fig. 13.13) results in a corresponding variation of $\gamma(t)$ that is sharply peaked. Returning to Einsteins theory of relativistic Doppler up shift one would therefore expect the up shifting process to be restricted to a timescale of the order of the temporal width of each γ -spike – substantially shorter than an optical half cycle – and the maximum up shift to take place when the Lorentz factor reaches its maximum γ_{max} . Since the emission of high harmonic orders only takes place

Fig. 13.14 Scaling of the highest harmonic with laser intensity. The data from the Vulcan laser experiments [32] clearly follows the γ^3 law for an oscillating surface



for large values of γ a sharp temporal localisation of the emitted harmonics results and the harmonic radiation is emitted in a burst on the timescale of attoseconds. As illustrated in Fig. 13.13, the temporal duration of the γ -spikes reduces for increasing intensity as $T_{Spike} \sim T_0/\gamma_{max}$ (with $T_0 = 2\pi/\omega_0$) [25]. The pulses of duration T_{Spike} are up-shifted and compressed by the factor of $4\gamma_{max}^2$ – familiar from the continuously moving relativistic mirror. As a result the harmonics are emitted in short temporal bursts with $T_{burst} \sim T_{Spike}/\gamma_{max}^2 \sim T_0/\gamma_{max}^3$ and hence, from Fourier-theory, must contain significant spectral components up to frequencies of $O \sim \omega_0 \gamma_{max}^3$. In effect, the high energy cut-off and the ultimate slope of the spectrum is governed by the temporal compression and truncation of the electromagnetic pulse rather than the maximum up shift expected from a relativistic mirror moving at constant γ . Experimental data (Fig. 13.14) obtained with the Vulcan laser shows that the highest harmonics observed follow the γ_{max}^3 trend – a powerful indication that the theoretical framework of ROM harmonics captures the essential physics correctly.

An estimate for magnitude γ_{max} can be obtained from the motion of a free electron in a laser field where $\gamma_{max} = (1 + 3.6 \times 10^{-19} I \lambda^2)^{1/2}$. Note that this applies only for gradients which are a significant fraction of the laser wavelength λ or greater. In the limit of very steep gradients the laser field at the surface is reduced and the higher plasma density leads to a larger restoring force. The influence of the peak plasma density in the limit of step-like density profiles can be quantified in terms of the similarity parameter $S = n_e/(a_0 n_c)$ [25, 33]. For constant S the surface dynamics of the plasma remain similar – particularly with regards to the velocity and phase of the ARP.

13.2.2.3 ROM Phase

In the previous section it was argued that the ultimate spectral extent of the ROM harmonics arise from temporal truncation of the up shifting process. This implies that the spectral phase of the highest harmonic orders must be constant or very close to constant (at least if we restrict the analysis to a single attosecond burst) and a pulse consisting of in the highest frequency part of the spectrum is therefore near transform limited. That this should be so, can be understood by a simple Gedanken experiment (thought experiment). If one takes a beam of light with a spectral width $\Delta\nu$ and truncates this to a duration Δt such that $\Delta\nu\Delta t \ll 1$ one obtains a beam with $\Delta\nu' \gg \Delta\nu$. The condition $\Delta\nu\Delta t \ll 1$ implies that Δt is much less than the coherence time $t_c \sim 1/\delta\nu$. The carrier oscillation within the time window Δt must therefore have full temporal coherence, i.e. flat spectral phase. This transform limited phase structure for the highest harmonics is predicted to result in pulses in the zeptosecond regime ($1 \text{ zs} = 10^{-21} \text{ s}$) [30] under ideal conditions.⁵ There are however contributions to both spatial and temporal phase that can lead to a departure from this ideal scenario. The peak plasma density in a step-like plasma gradient effectively changes the resonance frequency of the system. As in a simple harmonic oscillator the ratio of driving frequency to resonance frequency determines the relative phase of driver and oscillator. In the case of a plasma surface this can be parametrised by the S -parameter mentioned above [33] and if the S -parameter varies in time or space (as it certainly will given the dependence on the laser strength a_0) the phase will vary temporally and spatially. Spatially this leads to phase-front curvature while temporally this results in a change in the periodicity of the pulse train. A larger effect is the motion of the critical surface under the immense laser pressure ($P = I/c \approx \text{Gbar}$). This pressure leads to a deformation of the critical density surface and a continuous underlying motion into the target (hole boring). This effect also leads to a departure from perfect periodicity and hence spectral changes [34] as well as a red-shift of the spectrum due to the Doppler-effect [35]. Finally, the radial deformation (denting) determines the observed angular distribution of ROM harmonics [36]. Such effects affect the spectral shape, but do not affect the duration of each individual attosecond burst of radiation.

13.2.2.4 Single Attosecond Pulses

To date single attosecond pulses have not been achieved from SHHG interactions, though trains of attosecond pulses have been observed [37]. However, the principles established for HHG remain the same for SHHG. In particular for the ROM process,

⁵A $\tau = 300 \text{ zs}$ pulse corresponds to a spatial extent in propagation direction of $\Delta x = \tau c = 1$. Maintaining the integrity of the pulse front of such a small extent in the propagation direction would be extremely challenging.

the scaling of the highest harmonic is more rapid than for HHG ($\gamma^3 \propto I^{3/2}$) and the pulse to pulse separation in the attosecond pulse-train is greater (T_0 compared to $T_0/2$). Thus the requirements regarding the pulse-duration are more relaxed than for HHG. The much higher laser power required raises a laser-technological challenge of providing few-cycle pulse-duration *and* high intensity concurrently, with only the latest generation of laser based on OPCPA technology capable of such performance [38]. Polarisation dependence for ROM harmonic is somewhat different than for HHG [24]. For oblique incidence circular and linear polarisation have comparable efficiency, thus precluding polarisation gating. However at normal (near-normal) incidence the oscillating component of the laser-forces vanish (are suppressed) and polarisation gating becomes viable – albeit at some cost to overall efficiency of the process [39].

13.3 Conclusion

Converting intense optical laser radiation to high order harmonics of the incident laser light is an excellent means of achieving phase controlled spectra with large spectral width – and hence attosecond pulses. HHG in gaseous targets is a highly effective means of producing phase-locked spectra with a spectral width sufficient to support attosecond pulses and is the work-horse of attosecond science to date [3]. The only significant limitation is the relatively low single shot yields which are the result of challenging, time and space dependent phase matching considerations and, to a certain extent, practical difficulties in using lasers with extreme peak powers in the PW regime effectively for HHG due to geometrical constraints. However the relative ease and versatility of gas targets ensures that the development effort for HHG has not yet reached its conclusion and schemes such as QPM may yet substantially transform what is possible with this source of attosecond XUV pulses. SHHG in general and the ROM mechanism in particular has the potential to increase the pulse brightness of attosecond pulses by many orders of magnitude. While experimental results to date are very encouraging, SHHG poses substantial additional complications with respect to targetry.

References

1. R. Neutze et al., *Nature* **406**, 752–757 (2000)
2. P. Corkum, F. Krausz, *Nat. Phys.* **3**, 381 (2007)
3. F. Krausz, M. Ivanov, *Rev. Mod. Phys.* **81**, 163 (2009)
4. M. Nisoli, G. Sansone, *Prog. Quant. Electron.* **33**, 17 (2009)
5. T. Brabec, F. Krausz, *Rev. Mod. Phys.* **72**, 545 (2000)
6. S. Backus et al., *Rev. Sci. Instrum.* **69**, 1207 (1998)
7. G. Tsakiris et al., *New J. Phys.* **8**, 19 (2006)
8. P.B. Corkum, *Phys. Rev. Lett.* **73**, 1994 (1993)

9. M. Ammosov, N. Delone, V. Krainov, JETP **91**, 2008 (1986)
10. S.G. Preston et al., Phys. Rev. A **53**, R31 (1996)
11. M.V. Frolov et al., Phys. Rev. Lett. **100**, 173001 (2008)
12. H.J. Shin et al., Phys. Rev. A, **63**, 053407 (2001)
13. G. Sansone et al., Science **314**, 443 (2006)
14. P.B. Corkum et al., Opt. Lett. **19**, 1870 (1994); M. Ivanov et al., Phys. Rev. Lett. **74**, 2933 (1995)
15. K.S. Budil et al., Phys. Rev. A **48**, R3437 (1993)
16. E. Constant et al., Phys. Rev. Lett. **82**, 1668 (1999)
17. C.G. Durfee et al., Phys. Rev. Lett. **83**, 2187 (1999)
18. M. Lewenstein et al., Phys. Rev. A **49**, 2117 (1994)
19. M.C. Chen et al., Phys. Rev. Lett. **105**, 173901 (2010)
20. A. Paul et al., Nature **421**, 51 (2003)
21. A. Willner et al., Phys. Rev. Lett. **107**, 175002 (2011)
22. C. Thaur, F. Qur, J. Phys. B: At. Mol. Opt. Phys. **43**, 213001 (2010)
23. U. Teubner, P. Gibbon, Rev. Mod. Phys. **81**, 445 (2009)
24. R. Lichters, J. Meyer-ter-Vehn, A. Pukhov, Phys. Plasmas **3**, 3425 (1996)
25. T. Baeva et al., Phys. Rev. E **74**, 046404 (2006)
26. A. Einstein, Ann. Phys. (Leipzig) **17**, 891 (1905)
27. S.V. Bulanov, N.M. Naumova, F. Pegoraro, Phys. Plasmas **1**, 745 (1994)
28. P. Gibbon, Phys. Rev. Lett. **76**, 50 (1995)
29. P. Norreys et al., Phys. Rev. Lett. **76**, 1832 (1996)
30. S. Gordienko et al., Phys. Rev. Lett. **93**, 115002 (2004)
31. S. Gordienko et al., Phys. Rev. Lett. **94**, 103903 (2005)
32. B. Dromey et al., Phys. Rev. Lett. **99**, 085001 (2007)
33. D. an der Brügge, A. Pukhov, Phys. Plasmas **14**, 093104 (2007)
34. M. Behmke et al., Phys. Rev. Lett. **106**, 185002 (2011)
35. M. Zepf et al., Phys. Plasmas **3** 3242 (1996)
36. B. Dromey et al., Nat. Phys. **2**, 456 (2006).
37. Y. Nomura et al., Nat. Phys. **5**, 124 (2009)
38. F. Tavella et al., Opt. Lett. **32**, 2227 (2007)
39. S. Rykovanov et al., New J. Phys. **10**, 025025 (2008)